sustainability

MDPI

Article

Adaptive PI Control Strategy for Optimal Microgrid Autonomous Operation

Ahmed M. Hussien [1], Jonghoon Kim [2], Abdulaziz Alkuhayli [3], Mohammed Alharbi [3], Hany M. Hasanien [4,*], Marcos Tostado-Véliz [5], Rania A. Turky [1] and Francisco Jurado [5]

1 Electrical Engineering Department, Faculty of Engineering and Technology, Future University in Egypt, Cairo 11835, Egypt
2 Energy Storage and Conversion Laboratory, Department of Electrical Engineering, Chungnam National University, Daejeon 34134, Korea
3 Electrical Engineering Department, College of Engineering, King Saud University, Riyadh 11421, Saudi Arabia
4 Electrical Power and Machines Department, Faculty of Engineering, Ain Shams University, Cairo 11517, Egypt
5 Department of Electrical Engineering, Superior Polytechnic School of Linares, University of Jaén, 23700 Linares, Spain
* Correspondence: hanyhasanien@ieee.org

Abstract: The present research produces a new technique for the optimum operation of an isolated microgrid (MGD) based on an enhanced block-sparse adaptive Bayesian algorithm (EBSABA). To update the proportional-integral (PI) controller gains online, the suggested approach considers the impact of the actuating error signal as well as its magnitude. To reach a compromise result between the various purposes, the Response Surface Methodology (RSMT) is combined with the sunflower optimization (SFO) and particle swarm optimization (PSO) algorithms. To demonstrate the success of the novel approach, a benchmark MGD is evaluated in three different Incidents: (1) removing the MGD from the utility (islanding mode); (2) load variations under islanding mode; and (3) a three-phase fault under islanding mode. Extensive simulations are run to test the new technique using the PSCAD/EMTDC program. The validity of the proposed optimizer is demonstrated by comparing its results with those obtained using the least mean and square root of exponential method (LMSRE) based adaptive control, SFO, and PSO methodologies. The study demonstrates the superiority of the proposed EBSABA over the LMSRE, SFO, and PSO approaches in the system's transient reactions.

Keywords: adaptive control; enhanced block-sparse adaptive Bayesian algorithm; microgrid; response surface methodology

Citation: Hussien, A.M.; Kim, J.; Alkuhayli, A.; Alharbi, M.; Hasanien, H.M.; Tostado-Véliz, M.; Turky, R.A.; Jurado, F. Adaptive PI Control Strategy for Optimal Microgrid Autonomous Operation. *Sustainability* **2022**, *14*, 14928. https://doi.org/10.3390/su142214928

Academic Editor: George Kyriakarakos

Received: 15 October 2022
Accepted: 8 November 2022
Published: 11 November 2022

1. Introduction

1.1. Problem Understudy

To accommodate the spike in the load profile, decentralized renewable power networks are undergoing major reformation. These advancements have resulted in technical and scientific progress as well as environmental and economic advantages. Nevertheless, load demand is rising fast. This circumstance emphasizes the criticality of replacing centralized power plants with distributed generators (DGRs) placed over distribution networks [1]. This might be an effective countermeasure for reducing transmission losses and eliminating any need for extensive transmission networks. Some factors must be considered for the DGR units to supply the load continuously. As a result, the microgrid (MGD) concept arose as a set of DGRs and their associated loads in such a sub-network.

The MGDs are tiny conventional grids that may be operated and managed electrically in either grid-connected or grid-disconnected (islanded) mode [2]. The system point of common coupling (PCC) voltages and frequencies are identified by the utility in the grid-connected mode. Nonetheless, their active and reactive powers must be managed. In contrast, the microgrid's voltage and frequency must be modified in the islanded mode [3].

As a result, it is necessary to manage the DGR unit's functioning in order to supply the load continuously.

Different sophisticated control systems are used in islanded mode to ensure proper and reliable functioning. These control methods are classified into droop control (DPC), centralized, and multivariable and servomechanism (MAS) approaches. DPC provides peer-to-peer management and plug-and-play functionality by autonomously regulating the distinct DGR's outputs without requiring contact or communication among DGRs. A remote controller technique focused on active and reactive power DPC is suggested [4]. A fully decentralized method based on dual-frequency-droop control is proposed [5]. One of the profits of utilizing DPC is the capability to individualistically regulate scattered units without requiring contact between them. From the perspective of robustness and reliability, this technique beats previous power-sharing and MGD frequency-regulating methods. However, for lower voltage MGDs, line impedance significantly influences this control's efficiency, resulting in power conjugation [6]. The imaginary vectors conversion approach has been improved to avoid power conjugation [7]. However, it affects reliability. On the other hand, centralized control approaches need increased bandwidth linkages, and any break in those networks might cause a MGD collapse. A centralized control scheme for DC MGD built on independent communications was created and used [8]. Finally, a unique technique for creating multivariable robust servomechanism systems for several inputs and outputs and open-loop systems control is proposed [9]. Nevertheless, its immense complexity is a hindrance.

Because of its high stability margins, the proportional-integral (PI) controller has become the most commonly used controller for non-linear systems. However, it has difficulty dealing with parameter variation sensitivity and network nonlinearities. Consequently, identifying the proper PI configuration in this scheme is a significant challenge. In recent years, extensive studies have been conducted to develop the ideal controller for MGD controls to maintain a reliable system. In this aspect, PI controllers use a d-q frame to adjust the voltage of the voltage source converter [10]. Furthermore, whenever the system is assumed linear, PI controllers are tuned by simple procedures such as the Ziegler-Nichols method [11]. In contrast, the PI controller produces a saturated result, reducing the system stability due to a more significant phase lag. A decentralized PI controller for regulating a hybrid power scheme is introduced in [12]. As a result, several metaheuristic algorithms that simulate biological or physical events can resolve objective functions.

The metaheuristic algorithms are derived from natural phenomena such as animals, people, and physics [13], such as the Binary Chimp Optimization Algorithm (BCA) [14], the Heap optimization algorithm [15], the Sunflower (SFO) algorithm [16], the Aquila Optimizer algorithm (AO) [17], the Political Optimizer (PO) [18], the Archimedes algorithm [19], the Cuttlefish optimization algorithm (CFA) [20], and coot bird metaheuristic optimizer (CBMO) [11]. Several of these techniques have advantages and problems [21]. We are still far from having a global framework for the MGD scheme.

1.2. Literature Review

Although the optimization methodologies are efficient and robust tools for designing PI controllers, they have significant drawbacks, such as a complicated process, a considerable memory demand, and more time in the optimization procedure. As a result, the adaptive PI controller is a strong choice for tuning PI controller parameters online without any optimization methods. This reduces the time spent on the layout and the effort expended on this problem. In addition, several adaptation techniques were used to adjust the PI controller. Adaptive control (ACT) is introduced, depending on an affine projection algorithm with quicker convergence and fewer system complexities than optimization techniques [22]. It also displays some appealing elements, including the coefficient vector. Moreover, this strategy repeatedly approaches accurate data independent of the variables, as described in [23]. A novel ACT utilizing a set-membership engine algorithm outperforming existing strategies is presented [24]. In [25], the least mean (LM) and the

square root of exponential (SRE) techniques are presented as unique ACT. The use of an absolute negative error causes this approach to be normalized. LMSRE also offers quick convergence and reliability with minimum error. The proposed enhanced block-sparse adaptive Bayesian algorithm (EBSABA) outperforms conventional adaptive techniques [26]. The EBSABA's advantages include quick convergence, a straightforward technique, and decreased computing complexities. Furthermore, the suggested technique may consider the influence of the actuation mistake, its magnitude signal, and the sparse block method. This is the primary motivation for the authors to use this high-performance technique for live updating the PI controller gains of the DGRs.

This work adds to that pool by introducing a unique way for an optimum regulation of islanded MGDs based on the EBSABA. This study employs this adaptive technique in a PI controller optimum control strategy with multiple PI controller parameters to improve the efficiency of the off-grid mode process. To verify the proposed technique, several simulations are run to demonstrate the effectiveness of the proposed EBSABA in the system's transient responses over LMSRE-based ACT and specific other optimization strategies, such as the SFO and PSO approaches.

1.3. The Major Contribution

This research contributes to filling the gaps already revealed by:

(1) Testing the newly suggested EBSABA algorithm on customized PI controllers to boost MGD efficiency,

(2) Demonstrate the success of the novel approach by investigating the MGD under three altered operating states:

   (a) Removing the MGD from the utility (islanding mode);
   (b) Load variations under islanding mode; and
   (c) A three-phase fault under islanding mode,

(3) Demonstrate the strength of the presented adaptive technique by comparing its results with other optimization approaches.

This is how the article's remaining Sections are organized. Section 2 shows the MGD modeling. Section 3 describes the control scheme. Section 4 depicts the design processes. Section 5 represents the old optimization techniques and EBSABA modeling stages. Section 6 presents and discusses the simulation outputs. Finally, in Section 7, the conclusion is stated.

2. MGD Demonstrating

A MGD is shown in Figure 1, which has been primarily split into three DGRs connected by transmission lines. Transmission lines link the primary grid to the DGRs throughout PCC 1. To prevent unnecessary power quality difficulties, each DGR comprises a DC supply coupled to pulse width modulation (PWM) connected to a transformer through a filter. A complex load is added after the Δ-Y transformer. Table 1 has the MGD details.

Table 1. MGD information.

Transformer Data		**Δ/Y = 0.6/13.8 KV**
Load data	Load 1	C_1 = 50 μF, R_{l1} = 9 Ω, R_{l2} = 150 Ω, L_1 = 0.6 H
	Load 2	C_2 = 42 μF, R_{22} = 5 Ω, R_{l2} = 75 Ω, L_2 = 0.4 H
	Load 3	C_3 = 33 μF, R_{33} = 20 Ω, R_{l2} = 50 Ω, L_3 = 1.5 H
Transmission Line Parameters	Z_{TL1}	R_{TL1} = 0.7 Ω, L_{TL1} = 0.5 mH
	Z_{TL2}	R_{TL2} = 1.5 Ω, L_{TL2} = 0.9 mH
Filter data (Z_f)		R_f = 1.5 mΩ, X_f = 0.5 mH
Grid parameters		V = 13.8 KV, R_g = 0.2 Ω, L_g = 0.3 mH

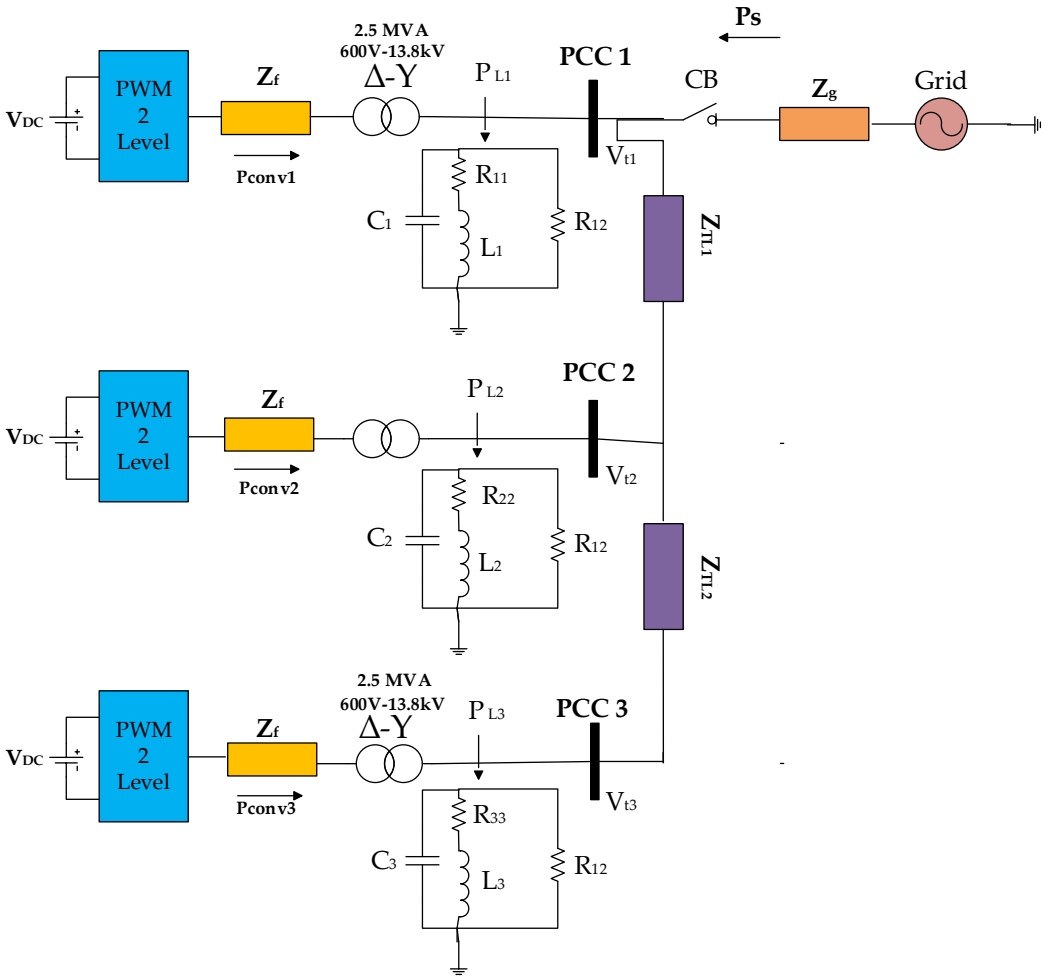

Figure 1. MGD diagram.

The proposed MGDs may be operated and managed electrically in either grid-connected or grid-disconnected (islanded) mode. The utility in the grid-connected mode identifies the PCC voltages and frequencies. Nonetheless, their active and imaginary powers must be managed. In contrast, the microgrid's voltage and frequency need to be modified in the islanded mode. As a result, it is necessary to address the DGR unit's functioning in order to supply the load continuously. This article concentrates on boosting the MGD efficiency in islanded mode by using the cascading control mechanism described in detail in the next section.

3. Control Scheme

The cascading control approach is utilized in every DGR with two control loops. In the grid-connected mode, the outer control loop regulates the real and imaginary powers (P, Q). At the same time, the direct and quadrature current components ($I_{conv.\_d}$, I_{conv_q}) are tuned by the inner loop to regulate the voltages of the PCCs. In the off-grid mode, both terminal voltage components (V_q, V_d) are regulated using the outer loop, while the Iconv_d and Iconv_q are tuned utilizing the inner control loop. The references voltages ($V_{conv.\_a}$*, $V_{conv.\_b}$*, $V_{conv.\_c}$*) are obtained via the transformation of the d-q references voltages ($V_{conv.\_d}$*, $V_{conv.\_q}$*). $V_{conv.\_d}$*and $V_{conv.\_q}$* are calculated using the four PIs presented in Figure 2. Finally, the inverter switches pulses using a comparator that matches a triangle signal at 1980 Hz (60 HZ pairs) to the reference voltages ($V_{conv.\_a}$*, $V_{conv.\_b}$*, $V_{conv.\_c}$*).

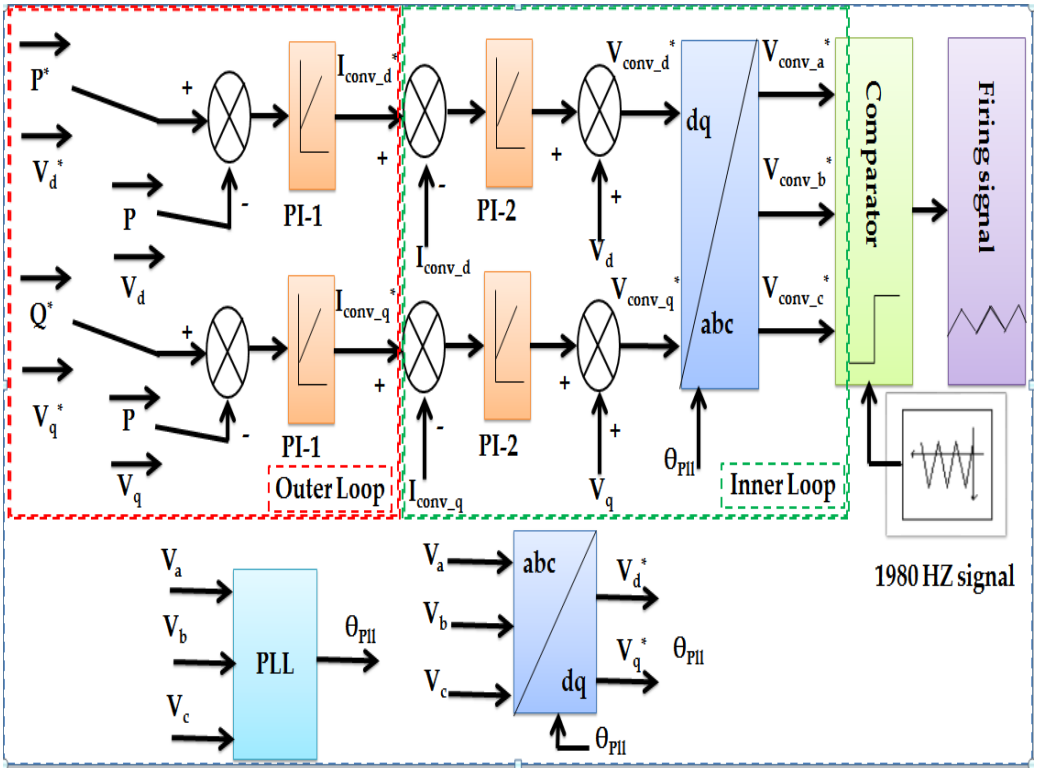

Figure 2. Control scheme for islanding MGD.

The EBSABA method and other approaches are used to calculate the gains of the four PI controllers. Section 4 delves more into this.

P is the actual active power of the converter, Q is the actual reactive power of the converter, I_{conv_d} is the direct axis component current of the inverter, I_{conv_q} is the quadrature axis component current of the inverter, V_d is the grid direct axis voltage, V_q is the grid quadrature axis voltage, I_d is the grid direct axis current, I_q is the grid quadrature axis current, and $V_{conv\cdot\_a}$*, $V_{conv\cdot\_b}$*, and $V_{conv\cdot\_c}$* are the three-phase inverter reference voltages Ia,b,c are the three-phase inverter voltages and currents.

4. Procedure for Designing

4.1. Gains Configuration

In this paper, two PIs are used in every DGR: PI_{11} and PI_{12} are PI controllers used in DGR_1, $PI_{21,}$ and PI_{22} are PI controllers used in DGR_2, and PI_{31} and PI_{32} are PI controllers used in DGR_3.

In this paper, the parameters of the PI controllers are proportional gain (KP) and integral time constants (TI), where: U_1 is the KP of the PI_{11}, U_2 is the TI of the PI_{11}, U_3 is the KP of the PI_{12}, ... , U_{11} is the KP of the PI_{32}, and U_{12} is the TI of the PI_{32}.

Table 2 displays the three levels used in this study for the controllers' parameters.

4.2. PSCAD/EMTDC Program

The MGD system is simulated using the PSCAD software. The data collected from these simulations in different circumstances is used as the RSMT's inputs.

4.3. RSMT & MINITAB Programs

The RSMT is a numerical tool that empirically generates solutions by employing a robust analytical method to find connections between the inputs and outputs [11]. The RSMT input signals are the steady-state error (Est), maximum percentages under and overshoots (MPUST and MPOST), and settling time (Tst) of the profile voltage, which

is taken from PSCAD and reported in [11]. The MINITAB software is used to design the RSMT.

Table 2. RSMT levels.

Gains Limits	(−1)	(0)	(1)
U_1	2.1	4.8	7.6
U_2	0.00085	0.007925	0.015
U_3	1.7	2.375	3.05
U_4	0.055	1.5775	3.1
U_5	1.6	4.4	7.2
U_6	0.00095	0.008225	0.0155
U_7	1.45	2	2.55
U_8	0.1	1.475	2.85
U_9	1.1	3.825	6.55
U_{10}	0.00095	0.005975	0.011
U_{11}	1.25	1.7	2.15
U_{12}	0.055	1.3275	2.6

Levels (−1), (0), (1): are the lowest, midpoint, and highest safe values.

The minimization of the MPOST (B1), MPUST (B2), Tst (B3), and Est (B4) for the specified circumstances defines the multi-objective function for this MGD. The second-order polynomial RSMT model is depicted in Equation (1).

$$B_i = S_1 + S_2U_1 + S_3U_2 + S_4U_3 + S_5U_4 + S_6U_1^2 + S_7U_2^2 + S_8U_3^2 + S_9U_4^2 + S_{10}U_1U_2 + S_{11}U_1U_3 + S_{12}U_1U_4 + S_{13}U_2U_3 + S_{14}U_2U_4 + S_{15}U_3U_4 \quad (1)$$

where i = 1, 2, 3, 4, and S_1, S_2, . . . , S_{15} are the estimated RSMT constants for the circumstances presented in [11].

5. Phase of Optimization

Equation (1) employs the weight approach [27] to the SFO and PSO procedures to optimize PI parameters while minimizing transients. Table 3 shows the utilized weights.

Table 3. Weights levels.

Weights (Wg)	DGR #		
Wg_1	DGR1	MPUST	0.19
Wg_2		MPOST	0.19
Wg_3		T_{st}	0.06
Wg_4		E_{st}	0.02
Wg_5	DGR2	MPUST	0.13
Wg_6		MPOST	0.13
Wg_7		T_{st}	0.05
Wg_8		E_{st}	0.015
Wg_9	DGR3	MPUST	0.08
Wg_{10}		MPOST	0.08
Wg_{11}		T_{st}	0.03
Wg_{12}		E_{st}	0.015

5.1. The SFO Algorithm

The fundamental motivation for adopting SFO in optimizing complex problems is the growth of soft computing capabilities. The SFO is an approach that is inspired by nature. Its primary concept is to mimic the arrangement of sunflowers (SFs) in order to collect sunlight [28]. The SF pattern is repetitive daily, beginning in the morning and ending at dusk. At dusk, the SF returns to its initial location in readiness for the sun to rise. It is believed that every SF has only one pollen gamete. In this Incident, emission from the

inverse square technique is crucial. SFs gather much of the sun's energy compared to those far away. In this position, the SFs facing the sun are calmer [28]. Equation (2) shows each group's energy storage [28].

$$E_s = \frac{H}{4\pi d_t^2} \tag{2}$$

where H signifies the source and d_t the spaces among the recent best and population i.

Equation (3) depicts the movement of SFs [29]:

$$\vec{Ni} = \frac{P^* - P_i}{||P^* - P_i||}, \; i = 1, 2, \ldots, \; n_p \tag{3}$$

Equation (4) represents the movement of SFs in path N:

$$S_N = C \; \times \; Z_i(P_i + P_{i-1}) \times ||P_i + P_{i-1}|| \tag{4}$$

where P and P* are the normal and best population, n_p is the population's number, C describes the inertial constant of the SFs, and $Z_i(||p_i + p_{i-1}||)$ is the pollen possibility. The limitation of these aspects is indicated in Equation (5):

$$R_{max} = \frac{||P_{max.} - P_{min.}||}{2 \times n_p} \tag{5}$$

$P_{max.}$ and $P_{min.}$ represent the boundaries. The following equation describes the next plant:

$$P \; \rightarrow_{i+1} = \; P \; \rightarrow_i + S_N \times \; N \; \rightarrow_i \tag{6}$$

The SFO outcomes were obtained from [26].

5.2. LMSRE Algorithm

As shown in Figure 3, adaptive filtering (AF) techniques are commonly employed to calculate the impulse response (IR) filter (J_0) parameter [25]. On the other hand, the input I_G is a Gaussian noise N_G that passes through an FIR filter. As a result, it is determined by the error (e_G) equation:

$$e_G = d_G - X_G^T J_G \tag{7}$$

$$d_G = X_0^T J_G + N_G \tag{8}$$

where N_G is the noise signal, X_G is the estimated weight vector, X_0 is the unknown weight vector, and d_G is the predicted signal.

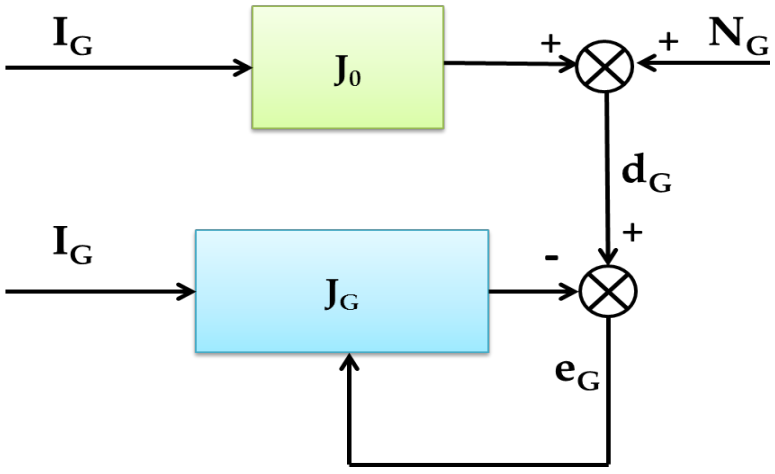

Figure 3. System prototypal of FIR filter.

Equation (9) shows that the AF algorithms are iterated utilizing a gradient approach [25]:

$$J_{G+1} = J_G - \mu \cdot \nabla_J \cdot T(J_G) \tag{9}$$

where G is the number of iterations, and J_G is the input vector. The gradient (∇_J) of the cost function (T) is then calculated using Equation (10):

$$\nabla_J T(J_G) = \text{sign}(e_G) \cdot (-I_G) - \left[\frac{\exp(-|e_G|)}{\sqrt{1+\exp(-|e_G|)}} \right] \tag{10}$$

Equation (7) is substituted into Equation (8) to get:

$$J_{G+1} = J_G - \mu_G \cdot \beta_G \cdot \text{sign}(e_G) \cdot I_G \tag{11}$$

where μ_G is configured to limit the errors, μ_G must be signed for a colossal error to allow for fast convergence. In contrast, μ_G must be lowered for minor errors. As a result, β_G deviates from [0, 1] and is reduced for little mistakes and vice versa. As a result, μ_G diverges in proportion to β_G specified in Equation (12):

$$\mu_G = \mu \cdot \beta_G^{\alpha-1} \tag{12}$$

where μ and α are constants in charge of μ_G's deviance. At that point, substituting Equation (11) for Equation (12) obtains:

$$J_{G+1} = J_G - \mu \cdot \beta_G^{\alpha} \cdot \text{sign}(e_G) \cdot I_G \tag{13}$$

The LMSRE technique alters PI Controller gains that employ Equation (13). The modified PI gains are as follows:

$$k_{p(G+1)} = k_{p(G)} + \Delta k_{p(G)} \tag{14}$$

$$T_{i(G+1)} = T_{i(G)} + \Delta T_{i(G)} \tag{15}$$

$$\Delta k_{p(G)} = \Delta T_{i(G)} = \mu \cdot \beta_G^{\alpha} \cdot \text{sign}(e_G) \cdot I_G \tag{16}$$

The initial PI gains for all PI controllers are manually determined by evaluating the system within its limits specified in Table 4. The LMSRE results were derived from [25].

Table 4. The opening PI parameters.

Gains	PI_{11}	PI_{12}	PI_{21}	PI_{22}	PI_{31}	PI_{32}
k_p	5.52	3.1	5.52	3.1	5.52	3.1
T_i	0.0031	0.31	0.0031	0.31	0.0031	0.31

5.3. EBSABA Algorithm

AF algorithms have been extensively utilized in various applications, including linear models, noise signal cancellation, digital communications networks, and data-driven monitoring [30]. An uncertain system may be sparse in the system identification issue, indicating that some IR variables are close to zero. Several methods for identifying sparse networks have been proposed [31]. The system IR of block-sparse (BS) systems includes multiple clusters with nonzero components. Well-known BS system examples are acoustic echo devices and satellite communications [29]. In addition, several techniques have been proposed in BS systems identification to minimize convergence time and improve algorithm resilience. For such applications, stochastic gradient descent techniques have been proposed [32].

A modern EBSABA is described in this paper. The Gaussian Markov model is used in the suggested technique to generate the unknown BS system. The suggested EBSABA

outperforms conventional adaptive algorithms such as LMS and resilient recursive algorithms in numerous ways. Among the benefits are rapid convergence, a straightforward technique, and less computing complexity. The suggested approach considers the impact of the actuating error signal, its magnitude, and the block sparse approach. In this case, the AF's actuating error (e_a) may be expressed as follows [26]:

$$e_a = d_a - X_a^T w_a \tag{17}$$

where d_a is the AF's output signal, X_a^T is the transposition of the input, and w_a is the AF's weight vector. The maximum posterior estimation method is employed to calculate the AF coefficient w. This is accomplished by maximizing the posterior probability Pp(w | d), which is described as follows:

$$P_P(w|d) = \frac{P_P(w)P_P(d|w)}{\sum_{w'} P_P(w')P_P(d|w')} \tag{18}$$

The following equation gives the maximum posterior estimation of w:

$$\hat{w} = \text{argmax}\, P_P(w)P_P(d|w) \tag{19}$$

$$P_P(d|w) = \frac{1}{\sqrt{2\pi\sigma_a^2}} \exp\left(-\frac{\left(d - X^T\hat{w}\right)^2}{2\sigma_a^2}\right) \tag{20}$$

Then Equation (17) may be applied as follows:

$$\hat{w} = \text{argmax}(\log P_P(w) + \log P_P(d|w)) \tag{21}$$

$$\hat{w} = \text{argmax}\, L(w) \tag{22}$$

$$L(w) = \log P_P(w_1) + \sum_{i=1}^{L-1} \log(P_P(w_{i+1}|w_i)) \; - \frac{\left(d - X^T\hat{w}\right)^2}{2\sigma_a^2} \tag{23}$$

The optimum solution of Equation (22) of the BSABA relying on the steepest ascending technique is expressed as follows:

$$w_{a+1} = w_a + \rho \frac{\partial L(w)}{\partial w}|_{w=w_a} \tag{24}$$

In Equation (24), ρ indicates the step size variable. As a result, the gradient of L(w) concerning w is described as follows:

$$\frac{\partial L(w)}{\partial w} = \frac{\partial}{\partial w}\log(P_p(w_1)) + \frac{\partial}{\partial w}\sum_{i=1}^{L-1}\log(P_P(w_{i+1}|w_i)) - \frac{1}{2\sigma_a^2}\frac{\partial}{\partial w}\left(d - X^T\hat{w}\right)^2 \tag{25}$$

As a result, Equation (24) may be modified as follows:

$$w_{a+1} = w_a - \rho(g(w_a) + a(w_a)\;) \tag{26}$$

$$a(w_a) = \frac{-X_a e_a}{\sigma_a^2} \tag{27}$$

$$g(w_a) = [g(w_{1,a}), g(w_{2,a}), \ldots\ldots, g(w_{L,a})]^{\;T} \tag{28}$$

Equation (29) expresses the equation $g(w_{i,a})$ for index i = 1, 2 . . . , L:

$$g(w_{i,a}) = \frac{\frac{Z1w_{i,a}}{\sigma_{off}^3}\exp\left(\frac{-w_{i,a}^2}{2\sigma_{off}^2}\right) + \frac{Z2w_{i,a}}{\sigma_{on}^3}\exp\left(\frac{-w_{i,a}^2}{2\sigma_{on}^2}\right)}{\frac{Z1}{\sigma_{off}}\exp\left(\frac{-w_{i,a}^2}{2\sigma_{off}^2}\right) + \frac{Z2}{\sigma_{on}}\exp\left(\frac{-w_{i,a}^2}{2\sigma_{on}^2}\right)} \quad (29)$$

A modern EBSABA is provided in this study. In addition, this AF algorithm's weighting factor iteration is outlined as follows:

$$w_{a+1} = w_a + \gamma_1 e_a X_a + \gamma_2 |e_a| X_a - \rho g(w_a) \quad (30)$$

where w_a is the current weight factor, w_{a+1} is the next weight variable vector, γ_1 and γ_2 are minuscule positive numbers of 0.001 and 0.002, respectively, and the constant ρ is 0.11. Finally, it is worth noting that the EBSABA method matches the LMS algorithm but with block sparse term penalties ($g(w_a)$). Furthermore, $\gamma_1 = p_g$, $\gamma_1 = 1 - p_g$, and p_g is the Gaussian Mixture Markov probability, which is 0.91. The factors σ_{on} and σ_{off} are set at 1 and 0.01, respectively. These are the most commonly utilized values for creating AF. In this research, all PI controller gains are continually updated live using Equation (30). In this regard, $k_p(n)$ and $T_i(n)$ of the PI controllers are continuously updated using the following equations:

$$k_p(n+1) = k_p(n) + \Delta k_p(n) \quad (31)$$

$$T_i(n+1) = T_i(n) + \Delta T_i(n) \quad (32)$$

The modified gains of the PI controller are stated by comparing Equations (30)–(32):

$$\Delta k_p(n) = \gamma_1 e(n) X(n) + \gamma_2 |e(n)| X(n) - \rho g\big(k_p(n)\big) \quad (33)$$

$$T_i \Delta k_i(n) = \gamma_1 e(n) X(n) + \gamma_2 |e(n)| X(n) - \rho g(k_i(n)) \quad (34)$$

where e(n) is the PI controller's input signal and X(n) is the actual instantaneous signal, an input signal to the comparator.

6. Description and Outcomes of the Simulations

This section is dedicated to establishing the outcomes to demonstrate the cogency and usefulness of the proposed control scheme using the EBSABA. The success of the proposed approach is measured primarily by its ability to retain the PCC voltages within the defined limits in various MGD operating Incidents. In addition, the simulation results show the controller scheme's sanity, which was obtained using the PSCAD software. To demonstrate the efficiency of the new EBSABA-based adaptive control, it is matched to the outcomes produced with the other optimizations described in [25]. In addition, a benchmark MGD is evaluated in three different Incidents: (1) removing the MGD from the utility (islanding mode); (2) load variations under islanding mode; and (3) a three-phase fault under islanding mode.

6.1. Incident 1 (Off-Grid Mode)

In the initial Incident, the MGD usually operates and is linked to the grid. At 2 s, the MGD is forcefully split from the grid (off-grid mode). Table 5 shows the optimal PI gains for the DGRs with EBSABA, LMSRE, PSO, and SFO techniques. Figure 4a–c show the DGR's voltages with EBSABA and the other methods. Figure 5a–c display the complex power in the DGRs with EBSABA, LMSRE, PSO, and SFO techniques. It is essential to keep in mind that the MPUST for the off-grid mode of the given approach is less than 8.5% in Figure 4a. Furthermore, the suggested controller's T_{st} is lowered to 37 ms according to the 2% criteria, and the E_{st} is 0.2%. As a result, the introduced optimizer provides the least overshoots, the fastest damping, and the most appropriate Est. It is worth noting that the EBSABA outperforms the LMSRE, PSO, and SFO approaches in MPUST, MPOST, Tst, and

Est, demonstrating the rigor, validity, and practicality of the proposed EBSABA over the LMSRE, PSO, and SFO techniques.

Table 5. The outcomes of the three DGRs for Incident 1 with EBSABA, LMSRE, PSO, and SFO techniques.

	EBSABA	**LMSRE**	**SFO**		**PSO**	
Incident 1 DGR 1						
Optimum size	online	online	U_1	6.421	U_1	2.1472
			U_2	0.0054	U_2	0.00572
			U_3	2.952	U_3	1.6791
			U_4	0.3472	U_4	0.3392
MPUST	8.21%	7.93%	12.93%		20.4%	
MPOST	0%	0%	0%		0%	
T_{st}	0.037 s	0.045 s	0.0343 s		0.0562 s	
E_{st}	0.2%	0.34%	0.37%		0.42%	
Incident 1 DGR 2						
Optimum size	online	online	U_5	5.982	U_5	1.5692
			U_6	0.0042	U_6	0.00431
			U_7	2.5082	U_7	1.2342
			U_8	0.299	Y_8	0.30572
MPUST	8.1%	7.82%	12.54%		20.21%	
MPOST	0%	0%	0%		0%	
T_{st}	0.0353 s	0.0424 s	0.0325 s		0.0554 s	
E_{st}	0.19 %	0.32%	0.36%		0.415%	
Incident 1 DGR 3						
Optimum size	online	online	U_9	5.5343	U_9	1.07
			U_{10}	0.00314	U_{10}	0.0034
			U_{11}	2.0991	U_{11}	0.995
			U_{12}	0.2479	U_{12}	0.259
MPUST	7.95%	7.64%	12.32%		20.05%	
MPOST	0%	0%	0%		0%	
T_{st}	0.03495 s	0.0418 s	0.0319 s		0.0551 s	
E_{st}	0.187%	0.312%	0.354%		0.408%	

6.2. Incident 2 (Load Variations under Islanding Mode)

In the second Incident, the MGD runs steadily in the islanding operation. The MGD is first designed with a complex load, as shown in Table 1. Then, R_{12} is raised to 300 Ω at t = 3 s and returned to its previous value of 150 Ω at t = 3.4 s. Table 6 shows the optimal PI gains for the DGRs with EBSABA, LMSRE, PSO, and SFO techniques. Figure 6a–c shows the DGR's voltages with EBSABA and the other methods. Figure 7a–c displays the complex power in the DGRs with EBSABA, LMSRE, PSO, and SFO techniques. It is essential to remember that the MPUST for the load variation Incident of the given approach is less than 0.5% in Figure 6a. Moreover, the suggested controller's T_{st} is lowered to zero seconds according to the 2% criteria, and the E_{st} is 0.21%. As a result, the presented optimizer provides the least overshoots, the fastest damping, and the most appropriate E_{st}. It is important to remember that in Figure 6a, the active power of DGR1 is lowered to 1.3 MW and effectively returned to the previous level at t = 3.4 s. Nevertheless, the powers of

the remaining DGRs' have faster damping and lower swings. It is worth noting that the EBSABA outperforms the LMSRE, PSO, and SFO approaches in MPUST, MPOST, Tst, and Est, proving the rigor, cogency, and practicality of the suggested EBSABA over the LMSRE, PSO, and SFO techniques.

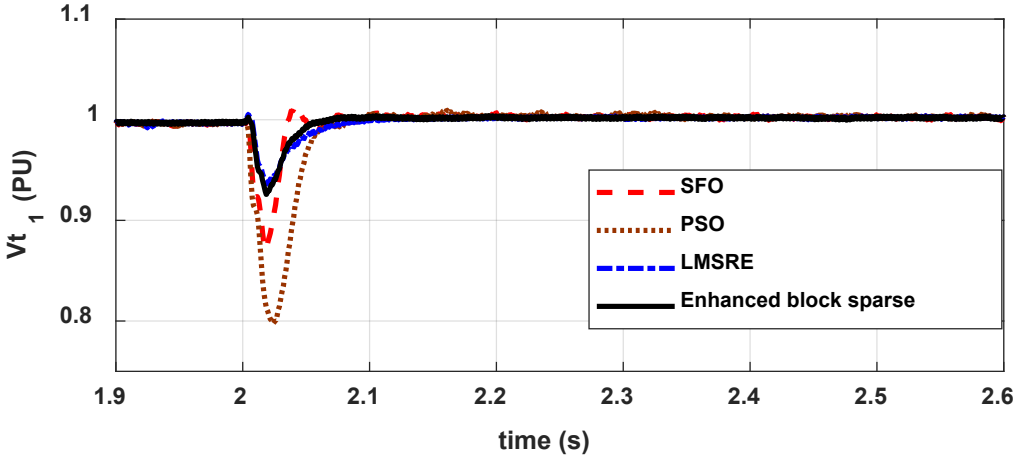

(**a**)

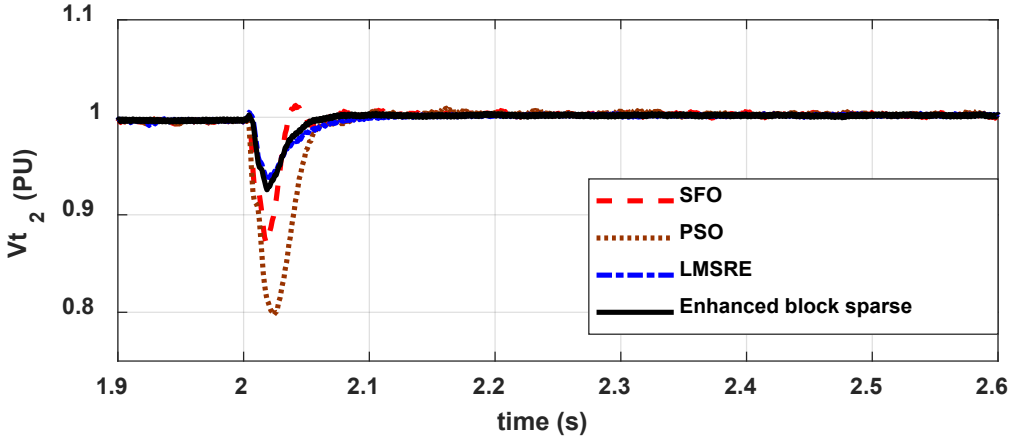

(**b**)

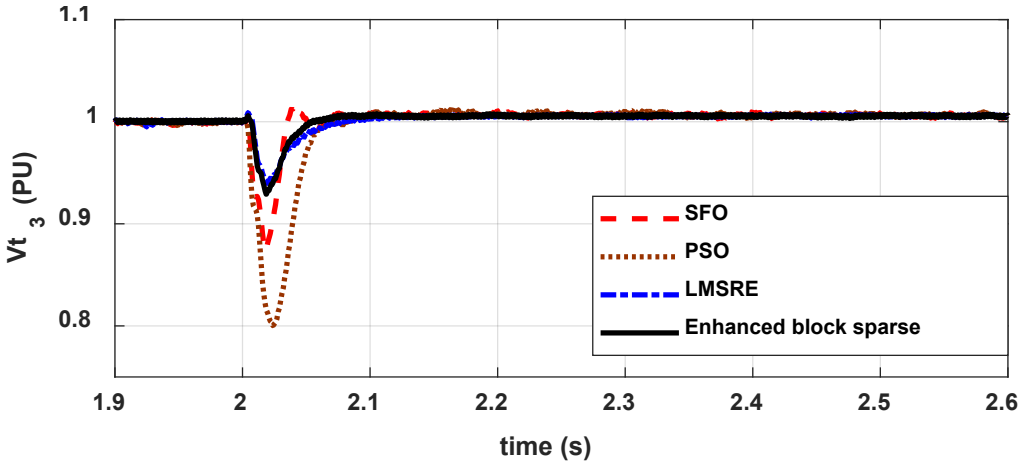

(**c**)

Figure 4. (**a**–**c**) The reference voltages for Incident 1 in the three DGRs with EBSABA, LMSRE, PSO, and SFO techniques.

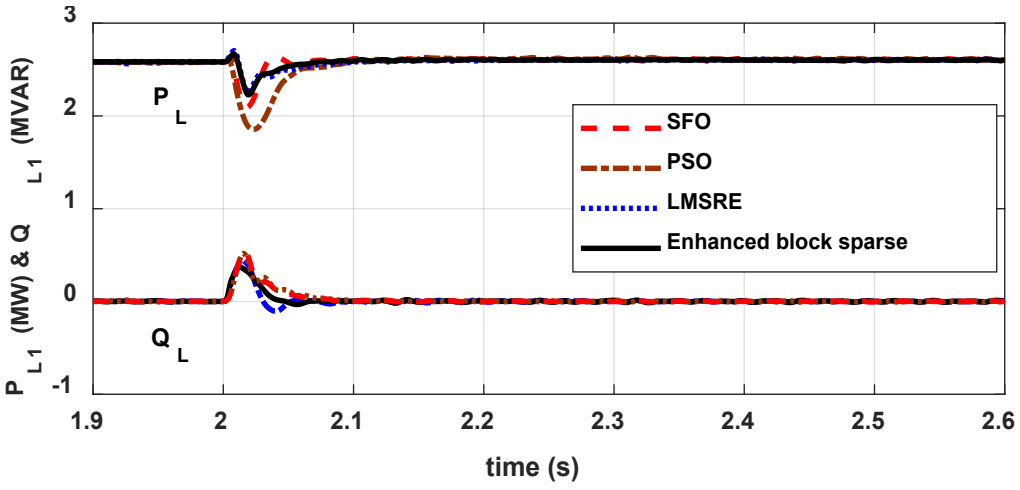

(**a**)

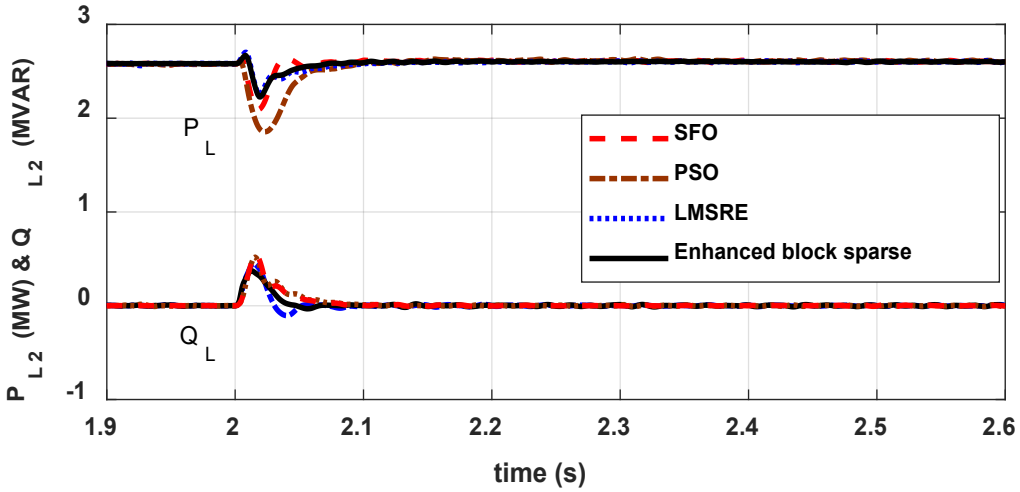

(**b**)

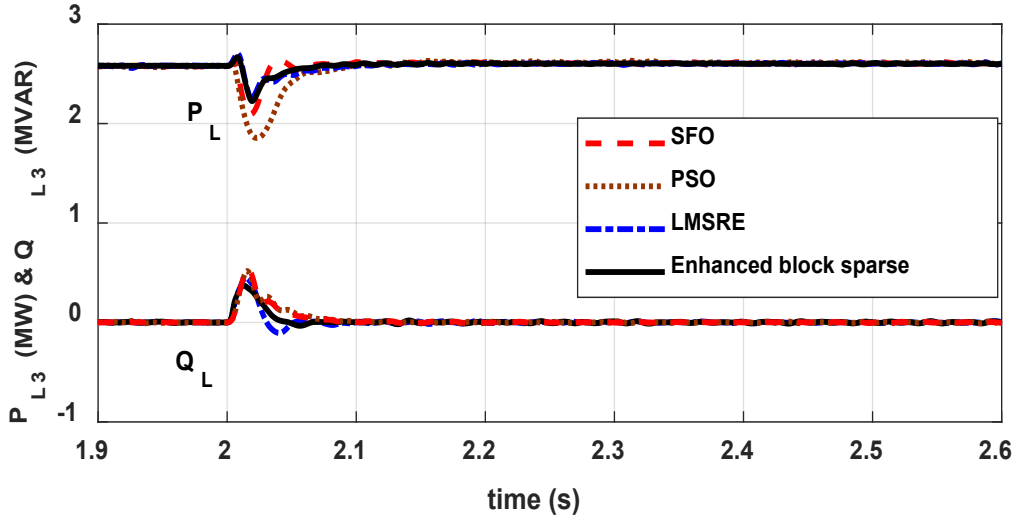

(**c**)

Figure 5. (**a**–**c**) The complex load powers for Incident 1 in the three DGRs with EBSABA, LMSRE, PSO, and SFO.

Table 6. The outcomes of the three DGRs for Incident 2 with EBSABA, LMSRE, PSO, and SFO techniques.

	EBSABA	**LMSRE**	**SFO**		**PSO**	
Incident 2 DGR 1						
Optimum size	online	online	U_1	6.469	U_1	1.924
			U_2	0.0125	U_2	0.0118
			U_3	2.2793	U_3	2.3123
			U_4	0.238	U_4	0.2315
MPUST	0.478%	1.91%	2.205%		3.27%	
MPOST	0.9745%	2.216%	2.967%		3.532%	
T_{st}	zero	0.4015 s	0.4331 s		0.453 s	
E_{st}	0.21%	0.425%	0.453%		0.496%	
Incident 2 DGR 2						
Optimum size	online	online	U_5	6.0246	U_5	1.4025
			U_6	0.0095	U_6	0.0103
			U_7	1.8614	U_7	1.7983
			U_8	0.2074	U_8	0.1999
MPUST	0.461%	1.821%	2.15%		3.234%	
MPOST	0.96%	2.202%	2.921%		3.457%	
T_{st}	zero	0.4003 s	0.4284 s		0.447 s	
E_{st}	0.203%	0.412%	0.441%		0.491%	
Incident 2 DGR 3						
Optimum size	online	online	U_9	5.4974	U_9	0.8995
			U_{10}	0.0069	U_{10}	0.0656
			U_{11}	1.5784	U_{11}	1.4879
			U_{12}	0.1753	U_{12}	0.1625
MPUST	0.454%	1.813%	2.07%		3.211%	
MPOST	0.952%	2.197%	2.906%		3.436%	
T_{st}	zero	0.3941 s	0.4233 s		0.418 s	
E_{st}	0.201%	0.403%	0.432%		0.486%	

6.3. Incident 3 (A Three-Phase Fault under Islanding Mode)

In Incident 3, the MGD runs steadily in the islanding operation. At t = 4 s, a three-phase fault occurs at PCC 1 and then returns to its previous case at t = 4.1 s. Table 7 shows the finest PI gains for the DGRs with EBSABA, LMSRE, PSO, and SFO techniques. Figure 8a–c shows the DGR's voltages with EBSABA and the other methods. Figure 9a–c displays the complex power in the DGRs with EBSABA, LMSRE, PSO, and SFO techniques. It is essential to keep in mind that in Figure 8a, the suggested controller's T_{st} is lowered to 22 ms according to the 2% criteria, and the Est is 0.19%. As a result, the introduced optimizer provides the least MPOST, the fastest damping, and the most appropriate Est. It is worth noting that the EBSABA outperforms the LMSRE, PSO, and SFO approaches in MPUST, MPOST, T_{st}, and E_{st}, proving the rigor, cogency, and practicality of the suggested EBSABA over the LMSRE, PSO, and SFO techniques.

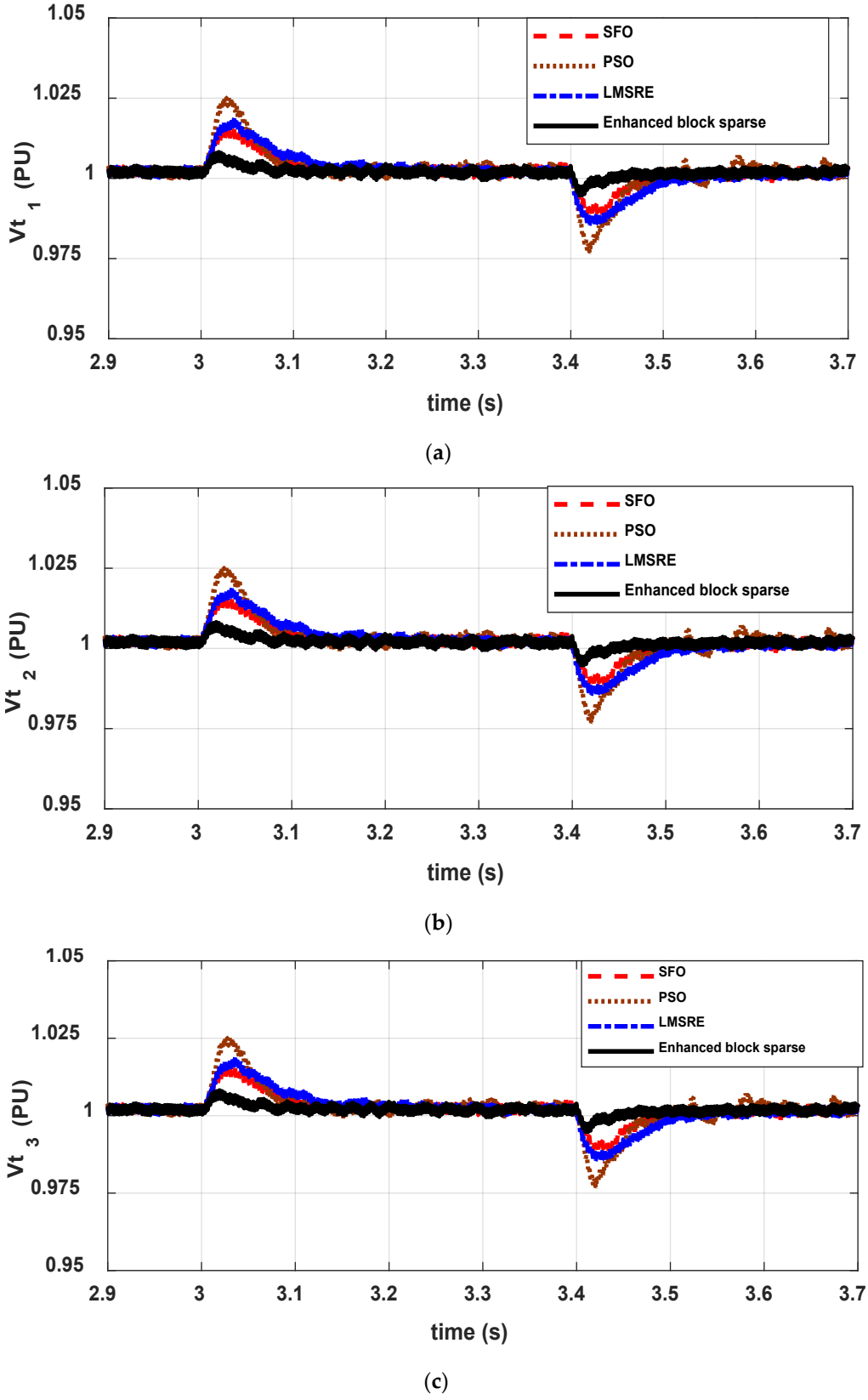

Figure 6. (**a**–**c**) The reference voltages for Incident 2 in the three DGRs with EBSABA, LMSRE, PSO, and SFO techniques.

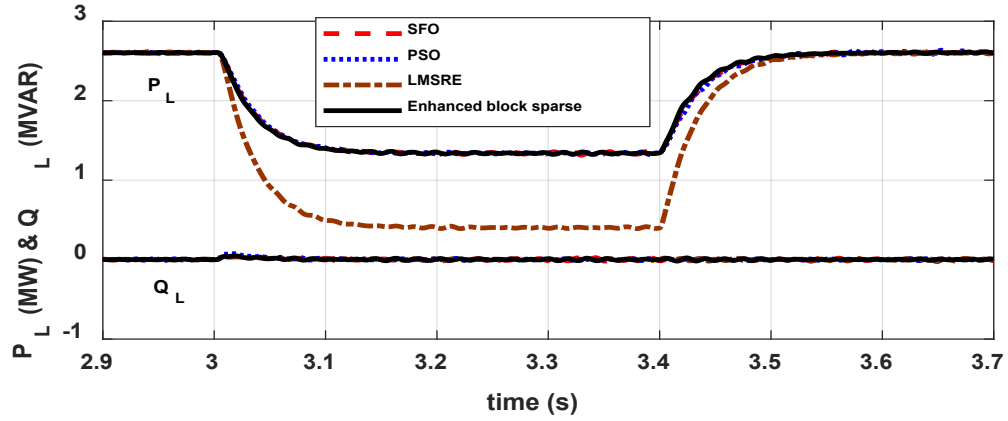

(**a**)

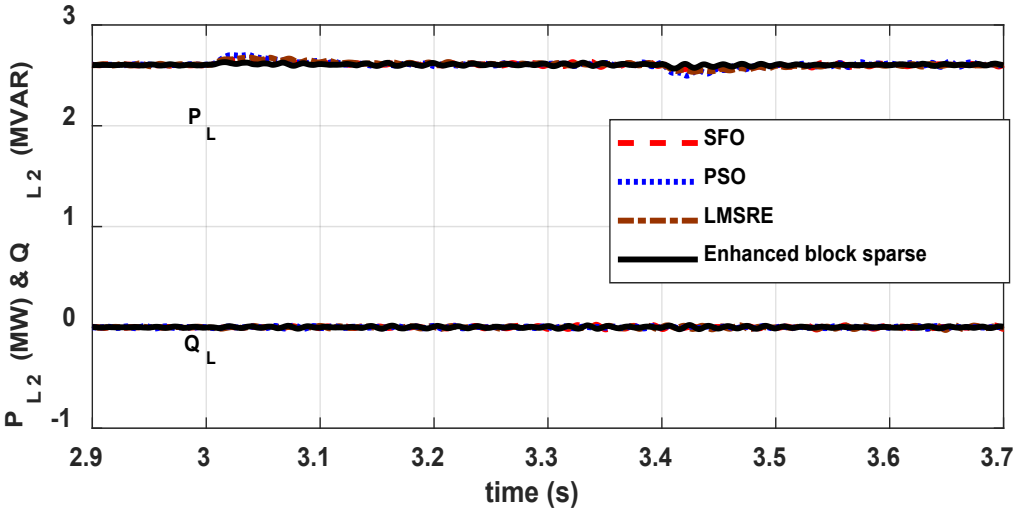

(**b**)

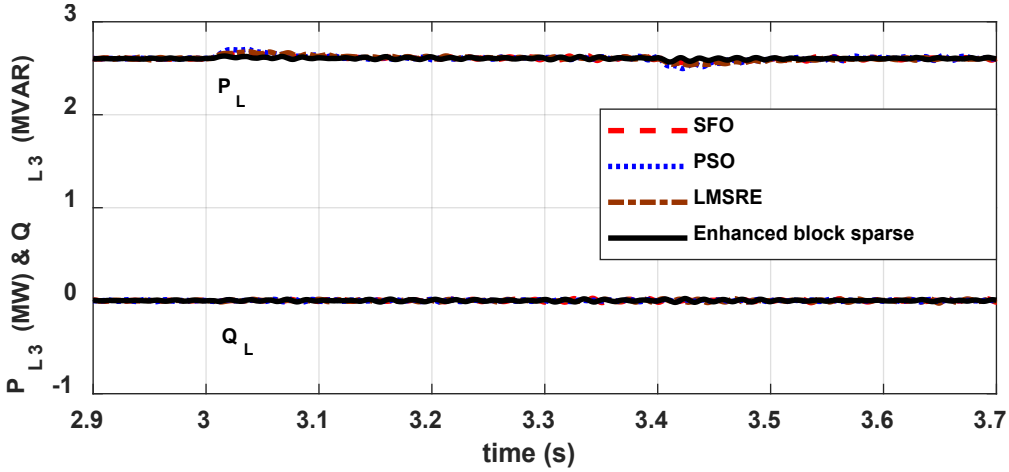

(**c**)

Figure 7. (**a**–**c**) The complex load powers for Incident 2 in the three DGRs with EBSABA, LMSRE, PSO, and SFO.

Table 7. The outcomes of the three DGRs for Incident 3 with EBSABA, LMSRE, PSO, and SFO techniques.

	EBSABA	**LMSRE**	**SFO**		**PSO**	
Incident 3 DGR 1						
Optimum size	online	online	U_1	6.1343	U_1	2.1084
			U_2	0.0045	U_2	0.0062
			U_3	2.4984	U_3	2.575
			U_4	0.1215	U_4	0.113
MPUST	92.05%	92.155%	91.65%		93.11%	
MPOST	10.5%	12.36%	11.69%		11.97%	
T_{st}	0.22 s	0.4912 s	0.566 s		0.812 s	
E_{st}	0.19%	0.257%	0.47%		0.549%	
Incident 3 DGR 2						
Optimum size	online	online	U_5	6.23	U_5	2.179
			U_6	0.0044	U_6	0.006
			U_7	2.515	U_7	2.554
			U_8	0.1193	U_8	0.099
MPUST	91.59%	92.07%	91.598%		93.09%	
MPOST	10.31%	12.31%	11.64%		11.89%	
T_{st}	0.214 s	0.488 s	0.556 s		0.806 s	
E_{st}	0.187%	0.2521%	0.4687%		0.546%	
Incident 3 DGR 3						
Optimum size	online	online	U_9	6.122	U_9	2.23
			U_{10}	0.0046	U_{10}	0.0063
			U_{11}	2.475	U_{11}	2.513
			U_{12}	0.1213	U_{12}	0.0108
MPUST	91.17%	91.86%	91.43%		92.88%	
MPOST	10.14%	12.22%	11.59%		11.83%	
T_{st}	0.212 s	0.483 s	0.551 s		0.795 s	
E_{st}	0.184%	0.25%	0.4679%		0.5423%	

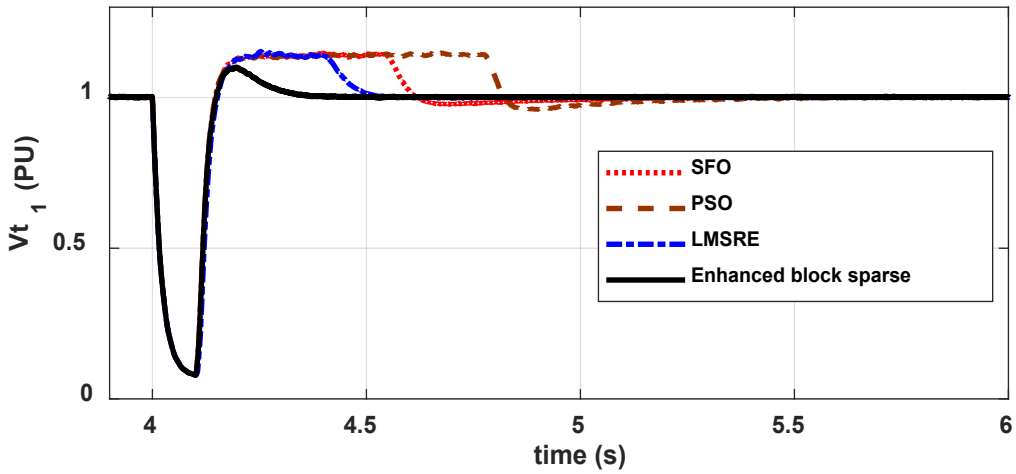

(**a**)

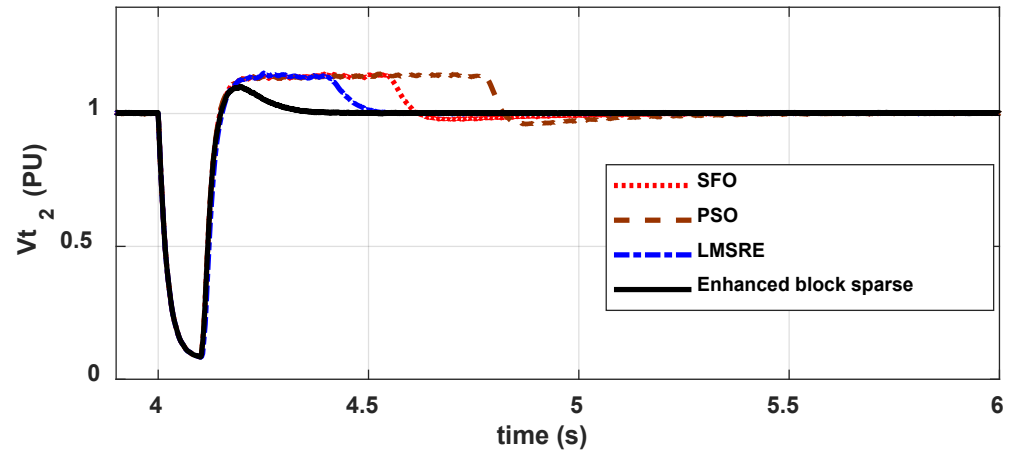

(**b**)

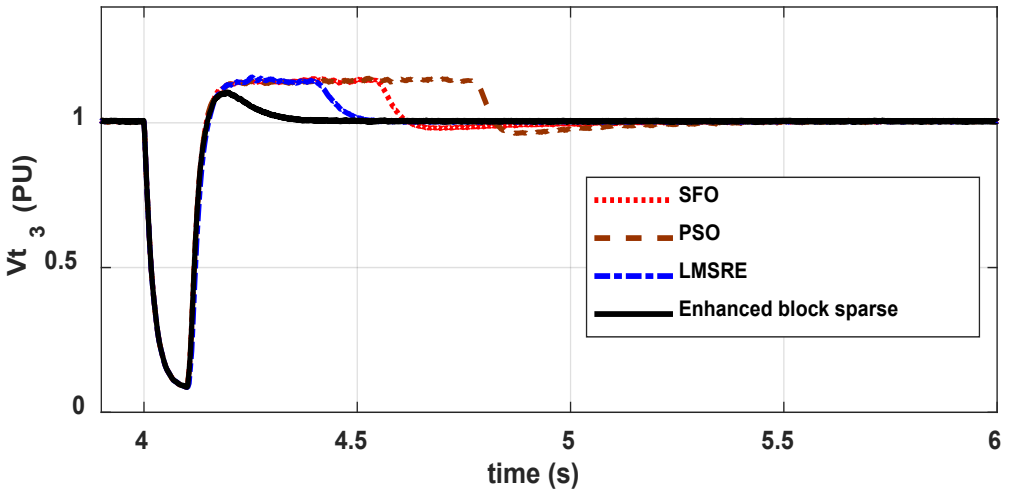

(**c**)

Figure 8. (**a**–**c**) The reference voltages for Incident 3 in the three DGRs with EBSABA, LMSRE, PSO, and SFO techniques.

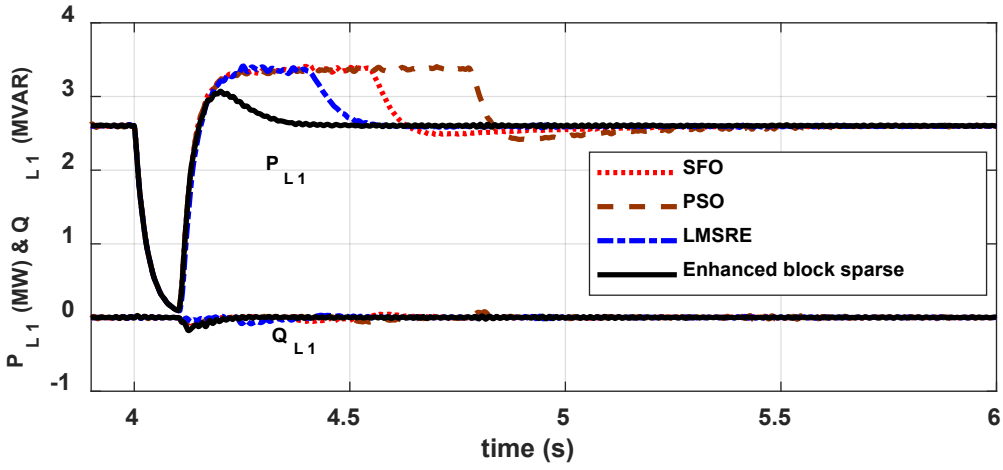

(**a**)

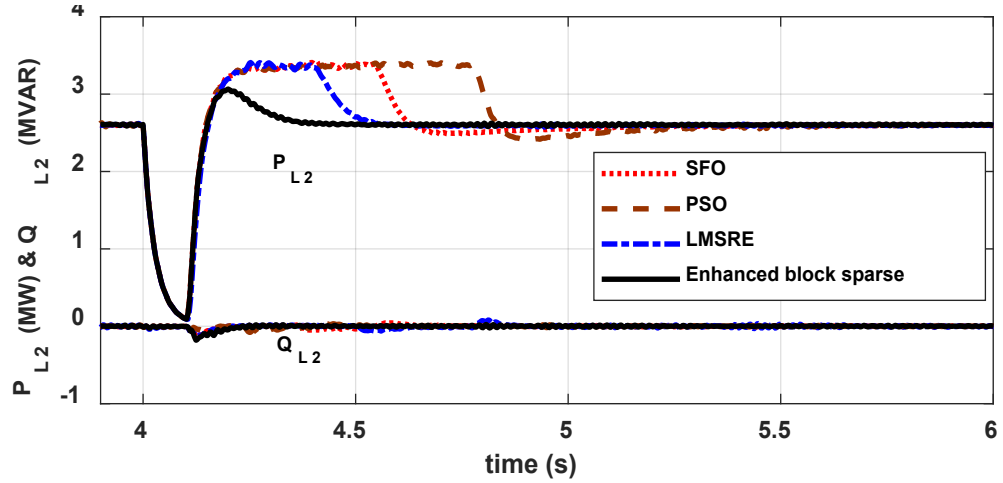

(**b**)

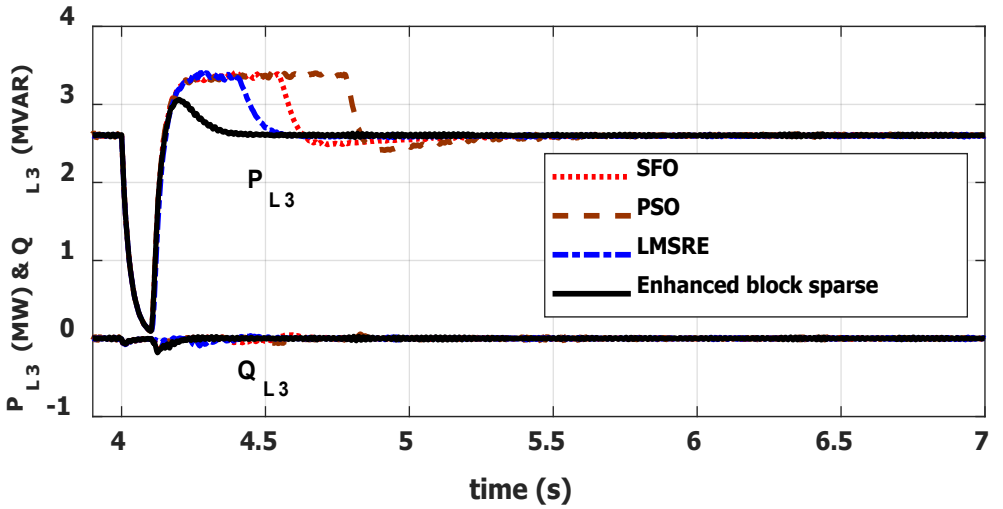

(**c**)

Figure 9. (**a**–**c**) The complex load powers for Incident 3 in the three DGRs with EBSABA, LMSRE, PSO, and SFO.

7. Conclusions

This research presents a novel PI controller optimum design based on EBSABA. To improve MGD efficiency, the proposed approach considers 12 PI controller gains. Two PI controllers are used for each DGR in the control approach. The simulation outcomes show the controller scheme's sanity, obtained using the PSCAD/EMTDC software. Furthermore, the results show that the suggested controller can maintain active and reactive powers while efficiently regulating the voltage profile. The outcomes data further indicated fast damping in the transient responses as well as a rapid Tst and a minor Est under multiple MGD operative Incidents: (1) removing the MGD from the utility (islanding mode); (2) load variations under islanding mode; and (3) a three-phase fault under islanding mode. To verify the proposed technique, several simulations are run to demonstrate the effectiveness of the proposed EBSABA in the system's transient responses over LMSRE-based adaptive control and specific other optimization strategies, such as the SFO and PSO approaches. More specifically, the EBSABA reduced the voltage MPUST by 75%, 78.3%, and 85.4% relative to the LMSRE, PSO, and SFO approaches. In Incident 2, when the MGD experienced a sudden change in the load under islanding mode, the proposed approach reduced Tst to zero seconds.

The future study will improve the proposed EBSABA to employ it in various applications such as power systems, energy storage techniques, and smart-grid, achieving the most satisfactory results in the clean energy schemes.

Author Contributions: A.M.H. and J.K.: conceptualization and methodology; A.A. and M.A.: validation, formal analysis; H.M.H. and M.T.-V.: investigation, visualization, supervision; R.A.T. and F.J.: review and editing. All authors have read and agreed to the published version of the manuscript.

Funding: This work was supported by the Researchers Supporting Project number (RSP2022R467), King Saud University, Riyadh, Saudi Arabia.

Institutional Review Board Statement: Not applicable.

Informed Consent Statement: Not applicable.

Data Availability Statement: Not applicable.

Acknowledgments: This work was supported by the Researchers Supporting Project number (RSP2022R467), King Saud University, Riyadh, Saudi Arabia.

Conflicts of Interest: The authors declare no conflict of interest.

Abbreviations

ACT	**Adaptive Control**
AF	Adaptive Filtering
AO	Aquila Optimizer
AVR	Automatic Voltage Regulator
BCA	Binary Chimp Optimization Algorithm
CBMO	Coot Bird Metaheuristic Optimizer
CFA	Cuttlefish Optimization Algorithm
DGR	Distributed Generator
DPC	Droop Control
EBSABA	Enhanced Block-Sparse Adaptive Bayesian Algorithm
EO	Equilibrium Optimization
E_{st}	Steady-State Error
GA	Genetic Algorithm
IR	Impulse Response
KP	Proportional Gain
LMSRE	Least Mean and Square Root of Exponential
MAS	Multivariable And Servomechanism

MGD	Microgrid
MPOST	Maximum Percentages Overshoot
MPUST	Maximum Percentages Undershoot
PCC	Point of Common Coupling
PI	Proportional-Integral
PO	Political Optimizer
PSO	Particle Swarm Optimization
PWM	Pulse Width Modulation
RSMT	Response Surface Methodology
SFO	Sunflower Optimization
TI	Integral Time Constant
T_{st}	Settling Time
ACT	Adaptive Control
Nomenclature	
B_1	Maximum Percentages Overshoot
B_2	Maximum Percentages Undershoot
B_3	Settling Time
B_4	Steady-State Error
C	the inertial constant of the SFs
d_a	is the AF's output signal
d_G	the predicted signal
d_t	the spaces among the recent best and population
E_s	the amount of energy stored
G	is the number of iterations
$g(w_a)$	block sparse term penalties
H	the source
i	Population number
J_0	the impulse response filter parameter
J_G	the input vector
N_G	the noise signal
n_p	the population's number
P	normal population
P*	best population
p_g	the Gaussian Mixture Markov probability
$P_{max.}$ and $P_{min.}$	the boundaries
$Pp(w \mid d)$	posterior probability
R_{max}	The limitation of the pollen possibility
$S_1, S_2, \ldots, S_{15}$	the estimated RSMT constants
S_N	the movement of SFs in path N
T	cost function
U_1 to U_{12}	the gains of the PI controllers
w	the AF coefficient
w_a	the AF's weight vector
X_a^T	the transpose of the input
X_0	the unknown weight vector
X_G	the estimated weight vector
$Z_i(\|\|p_i + p_{i-1}\|\|)$	the pollen possibility
∇	The gradient
μ_G	Error limiter
μ and α	Constants in charge of μ_G's deviance

References

1. Tabar, V.S.; Abbasi, V. Energy management in microgrid with considering high penetration of renewable resources and surplus power generation problem. *Energy* **2019**, *189*, 116264. [CrossRef]
2. Alghamdi, B.; Cañizares, C. Frequency and voltage coordinated control of a grid of AC/DC microgrids. *Appl. Energy* **2022**, *310*, 118427. [CrossRef]
3. Uddin, M.; Romlie, M.F.; Abdullah, M.F.; Tan, C.K.; Shafiullah, G.M.; Bakar, A.H.A. A novel peak shaving algorithm for islanded microgrid using battery energy storage system. *Energy* **2020**, *196*, 117084. [CrossRef]

4. Gaonkar, D.N.; Guerrero, J.M. Improved P-f/Q-V and P-V/Q-f droop controllers for parallel distributed generation inverters in AC microgrid. Sustain. *Cities Soc.* **2018**, *41*, 421–442. [CrossRef]
5. An, R.; Liu, Z.; Liu, J.; Liu, B. A Comprehensive Solution to Decentralized Coordinative Control of Distributed Generations in Islanded Microgrid Based on Dual-Frequency-Droop. *IEEE Trans. Power Electron.* **2022**, *37*, 3583–3598. [CrossRef]
6. Ozkan, Z.; Hava, A.M. Inductor Saturation Compensation in Three-Phase Three-Wire Voltage-Source Converters Via Inverse System Dynamics. *IEEE Trans. Ind. Electron.* **2022**, *69*, 4309–4319. [CrossRef]
7. D'Arco, S.; Suul, J.A.; Fosso, O.B. Automatic Tuning of Cascaded Controllers for Power Converters Using Eigenvalue Parametric Sensitivities. *IEEE Trans. Ind. Appl.* **2015**, *51*, 1743–1753. [CrossRef]
8. Saleh, M.; Esa, Y.; Mohamed, A. Centralized control for DC microgrid using finite state machine. In Proceedings of the 2017 IEEE Power & Energy Society Innovative Smart Grid Technologies Conference (ISGT), Washington, DC, USA, 23–26 April 2017. [CrossRef]
9. Wang, W.S.W.; Davison, D.E.; Davison, E.J. Controller design for multivariable linear time-invariant unknown systems. *IEEE Trans. Automat. Contr.* **2013**, *58*, 2292–2306. [CrossRef]
10. Bhateshvar, Y.K.; Mathur, H.D. Power–frequency balance with superconducting magnetic energy storage using optimized intelligent controller. *Energetika* **2014**, *60*, 149–161. [CrossRef]
11. Hussien, A.M.; Turky, R.A.; Alkuhayli, A.; Hasanien, H.M.; Tostado-Véliz, M.; Jurado, F.; Bansal, R.C. Coot Bird Algorithms-Based Tuning PI Controller for Optimal Microgrid Autonomous Operation. *IEEE Access* **2022**, *10*, 6442–6458. [CrossRef]
12. Patel, S.; Mohanty, B.; Hasanien, H.M. Competition over resources optimized fuzzy TIDF controller for frequency stabilization of hybrid micro-grid system. *Int. Trans. Electr. Energy Syst.* **2020**, *30*, e12513. [CrossRef]
13. Boussaïd, I.; Lepagnot, J.; Siarry. A survey on optimization metaheuristics. *Inf. Sci.* **2013**, *237*, 82–117. [CrossRef]
14. Wang, J.; Khishe, M.; Kaveh, M.; Mohammadi, H. Binary Chimp Optimization Algorithm (BChOA): A New Binary Meta-heuristic for Solving Optimization Problems. *Cognit. Comput.* **2021**, *13*, 1297–1316. [CrossRef]
15. Shaheen, M.A.M.; Hasanien, H.M.; Al-Durra, A. Solving of optimal power flow problem including renewable energy resources using HEAP optimization algorithm. *IEEE Access* **2021**, *9*, 35846–35863. [CrossRef]
16. Hussien, A.M.; Hasanien, H.M.; Mekhamer, S.F. Sunflower optimization algorithm-based optimal PI control for enhancing the performance of an autonomous operation of a microgrid. *Ain Shams Eng. J.* **2021**, *12*, 1883–1893. [CrossRef]
17. Abualigah, L.; Yousri, D.; Elaziz, M.A.; Ewees, A.A.; Al-qaness, M.A.A.; Gandomi, A.H. Aquila Optimizer: A novel meta-heuristic optimization algorithm. *Comput. Ind. Eng.* **2021**, *157*, 107250. [CrossRef]
18. Askari, Q.; Younas, I.; Saeed, M. Political Optimizer: A novel socio-inspired meta-heuristic for global optimization. *Knowledge-Based Syst.* **2020**, *195*, 105709. [CrossRef]
19. Hashim, F.A.; Hussain, K.; Houssein, E.H.; Mabrouk, M.S.; Al-Atabany, W. Archimedes optimization algorithm: A new metaheuristic algorithm for solving optimization problems. *Appl. Intell.* **2021**, *51*, 1531–1551. [CrossRef]
20. Hussien, A.M.; Mekhamer, S.F.; Hasanien, H.M. Cuttlefish Optimization Algorithm based Optimal PI Controller for Performance Enhancement of an Autonomous Operation of a DG System. In Proceedings of the 2020 2nd International Conference on Smart Power & Internet Energy Systems (SPIES), Bangkok, Thailand, 15–18 September 2020; pp. 293–298. [CrossRef]
21. Chaib, A.E.; Bouchekara, H.R.E.H.; Mehasni, R.; Abido, M.A. Optimal power flow with emission and non-smooth cost functions using backtracking search optimization algorithm. *Int. J. Electr. Power Energy Syst.* **2016**, *81*, 64–77. [CrossRef]
22. Wang, X.; Han, J. Affine projection algorithm based on least mean fourth algorithm for system identification. *IEEE Access* **2020**, *8*, 11930–11938. [CrossRef]
23. Lim, J.S. New adaptive filtering algorithms based on an orthogonal projection of gradient vectors. *IEEE Signal Process. Lett.* **2000**, *7*, 314–316. [CrossRef]
24. Werner, S.; Diniz, S.R. Set-membership affine projection algorithm. *IEEE Signal Process. Lett.* **2001**, *8*, 231–235. [CrossRef]
25. Hussien, A.M.; Turky, R.A.; Hasanien, H.M.; Al-Durra, A. LMSRE-based adaptive pi controller for enhancing the performance of an autonomous operation of microgrids. *IEEE Access* **2021**, *9*, 90577–90586. [CrossRef]
26. Hasanien, H.M.; Turky, R.A.; Tostado-Véliz, M.; Muyeen, S.M.; Jurado, F. Enhanced block-sparse adaptive Bayesian algorithm based control strategy of superconducting magnetic energy storage units for wind farms power ripple minimization. *J. Energy Storage* **2022**, *50*, 104208. [CrossRef]
27. Kim, I.Y.; de Weck, O.L. Adaptive weighted sum method for multiobjective optimization: A new method for Pareto front generation. *Struct. Multidiscip. Optim.* **2005**, *31*, 105–116. [CrossRef]
28. Shaheen, M.A.M.; Hasanien, H.M.; Mekhamer, S.F.; Talaat, H.E.A. Optimal power flow of power systems including distributed generation units using sunflower optimization algorithm. *IEEE Access* **2019**, *7*, 109289–109300. [CrossRef]
29. Das, B.K.; Chakravarthi, G.V.; Chakraborty, M. A Convex Combination of NLMS and ZA-NLMS for Identifying Systems with Variable Sparsity. *IEEE Trans. Circuits Syst. II Express Briefs* **2017**, *64*, 1112–1116. [CrossRef]
30. Habibi, Z.; Zayyani, H. Markovian Adaptive Filtering Algorithm for Block-Sparse System Identification. *IEEE Trans. Circuits Syst. II Express Briefs* **2021**, *68*, 3032–3036. [CrossRef]
31. Yoo, J.; Shin, J.; Park, P. An improved NLMS algorithm in sparse systems against noisy input signals. *IEEE Trans. Circuits Syst. II Express Briefs* **2015**, *62*, 271–275. [CrossRef]
32. Zhang, A.; Liu, P.; Sun, J.; Ning, B. Block-sparsity log-sum-induced adaptive filter for cluster sparse system identification. *IEEE Access* **2020**, *8*, 175265–175276. [CrossRef]